CHEMISTRY OF MATERIALS

Article

NaBiVO and KBiVO: New Lead-free Tetragonal Perovskites with Moderate *c/a* ratio

Hajime Yamamoto, Takahiro Ogata, Satyanarayan Patel, Jurij Koruza, Juergen Roedel, Atanu Paul, Tanusri Saha-Dasgupta, Yuki Sakai, Mitsuru Itoh, and Masaki Azuma

Chem. Mater., **Just Accepted Manuscript** • DOI: 10.1021/acs.chemmater.8b02379 • Publication Date (Web): 05 Sep 2018

$Na_{1/2}Bi_{1/2}VO_3$ and $K_{1/2}Bi_{1/2}VO_3$: New Lead-free Tetragonal Perovskites with Moderate *c*/*a* ratio

Hajime Yamamoto[†,*,○], Takahiro Ogata[†], Satyanarayan Patel[Δ], Jurij Koruza[Δ], Jürgen Rödel[Δ,+], Atanu Paul[#], Tanusri Saha-Dasgupta[#], Yuki Sakai[|], Mitsuru Itoh[†], and Masaki Azuma[†,*]

[†]Laboratory for Materials and Structures, Tokyo Institute of Technology, Yokohama, 226-8503, Japan

[Δ]Institute of Materials Science, Technische Universität Darmstadt, Darmstadt 64287, Germany

[+]Tokyo Tech World Research Hub Initiative (WRHI), Institute of Innovative Research, Tokyo Institute of Technology, Yokohama 226-8503, Japan

#Indian Association for the Cultivation of Science, Kolkata 700032, India

[|]Kanagawa Institute of Industrial Science and Technology, Ebina, Kanagawa 243-0435, Japan

ABSTRACT: New lead-free tetragonal perovskites $Na_{1/2}Bi_{1/2}VO_3$ and $K_{1/2}Bi_{1/2}VO_3$ were synthesized at high pressure and high temperature condition of 6 GPa and 1473 K, based on the materials design optimizing the lone pair effect of *A*-site ion and utilizing the Jahn-Teller effect in the *B*-site V^{4+}. The magnitudes of *c*/*a* ratio and spontaneous polarization, P_S, were *c*/*a* = 1.085 and P_S = 108 μC/cm² (73 μC/cm² by point charge model) for $Na_{1/2}Bi_{1/2}VO_3$ and *c*/*a* = 1.054 and P_S = 92 μC/cm² (56 μC/cm² by point charge model) for $K_{1/2}Bi_{1/2}VO_3$, which are comparable to the well-known lead-based ferroelectric $PbTiO_3$. The present approach can guide the design of new lead-free ferroelectric and piezoelectric materials.

1. INTRODUCTION

Polar tetragonal perovskites find potential applications in piezoelectric and pyroelectric devices, such as actuators and sensors. The most well-known representatives among them are compositions based on $PbTiO_3$, for example the widely-used piezoelectric material $PbZr_{1-x}Ti_xO_3$ (PZT). The compositions near the morphotropic phase boundary (MPB), separating the tetragonal phase on the $PbTiO_3$ side and the rhombohedral phase on the $PbZrO_3$ side, feature outstanding piezoelectric properties.[1-3] $PbTiO_3$ has a tetragonal structure (space group *P*4*mm*) with *c*/*a* ratio of 1.065 at room temperature.[4, 5] Both, Pb^{2+} ion at the *A*-site and Ti^{4+} at the *B*-site of the perovskite ABO_3 unit cell, contribute to the large distortion. The stereo-chemical activity of the Pb 6*s*² lone pair and the Pb-O covalency result in polar structures.[6, 7] The Ti^{4+} with 3*d*⁰ electron configuration is displaced off-center because of the hybridization of O 2*p* and empty Ti 3*d* orbitals, referred to as the "second-order Jahn-Teller effect".[8] The Ti-O polyhedron is a five-coordinate pyramid rather than a six-coordinate octahedron.

Because of the toxicity of lead, there is a growing interest in the quest for new lead-free piezoelectric materials that could replace PZT.[9, 10] Lead-free piezoelectrics were extensively studied in the last decade and many candidates have been reported, including perovskites based on $K_{1-x}Na_xNbO_3$ (KNN),[11] $Na_{1/2}Bi_{1/2}TiO_3$ (NBT),[12] $(Ba_{1-x}Ca_x)(Zr_{1-y}Ti_y)O_3$ (BCZT),[13] and $BiFeO_3$.[14-16] However, despite promising properties, PZT is still the predominantly used material in applications, due to the low production cost, high chemical stability, and high performance. The search for new lead-free piezoceramics often mimics the success of PZT, where a morphotropic phase boundary is formed between a rhombohedral and a tetragonal end members. This approach has been limited as only two lead-free tetragonal end members form at ambient pressure, namely $BaTiO_3$ and $K_{1/2}Bi_{1/2}TiO_3$.[10]

Bismuth-based perovskites are attractive candidates for lead-free piezoelectric materials, due to the low cost, non-toxic nature, and similar chemical properties of Pb and Bi. For example, the Bi^{3+} 6*s*² lone pair also exhibits stereo-chemical activity, which enables increased polarizability and unit cell distortion.[17] $PbTiO_3$-type bismuth-based perovskites, including $BiCoO_3$ (*c*/*a* = 1.27, P_S = 126 μC/cm²),[18, 19] Bi_2ZnTiO_6 (*c*/*a* = 1.21, P_S = 103 μC/cm²),[20] and Bi_2ZnVO_6 (*c*/*a* = 1.26, P_S = 126 μC/cm²),[21] have recently been found. The giant spontaneous polarization inhibits the polarization reversal and appearance of large piezoelectric response.[22, 23] Chemical substitution in Bi_2ZnTiO_6, such as La^{3+} for Bi^{3+}, $Mg^{2+}$for Zn^{2+}, and $Mn^{4+}$for Ti^{4+}, have been attempted to reduce the spontaneous polarization.[24-26] However, the magnitudes of spontaneous polarization hardly decreased in the tetragonal phases of $Bi_{2-x}La_xZnTiO_6$ (x < 0.3) and Bi_2Zn_{1-}

$_x$Mg$_x$TiO$_6$ (x < 0.3). The crystal structure changed to monoclinic *Ia* (*Cc*) phase in $Bi_2ZnTi_{1-x}Mn_xO_6$ ($0.2 \leqq x \leqq 0.45$). The spontaneous polarization barely decreased despite the reduced pseudo c/a ratio of 1.065 in $Bi_2ZnTi_{0.6}Mn_{0.4}O_6$ (P_S = 95.8 μC/cm²). The large atomic displacements in the BO_6 octahedron preserved the large spontaneous polarization in $BiZnTi_{1-x}Mn_xO_6$. Such a trend is also observed in $BiCo_{1-x}Fe_xO_3$. The giant spontaneous polarization was preserved in the tetragonal and monoclinic *Cm* phases in both bulk and thin film samples.[23, 27, 28]

$PbVO_3$ has a tetragonal structure with space group *P4mm*. The c/a ratio and spontaneous polarization reach 1.23 and 101 μC/cm², respectively.[29] The stereo-chemical activity of Pb^{2+} and strong Pb-O covalency stabilize the tetragonal structure, as in $PbTiO_3$. The V^{4+} ion with $3d^1$ electronic configuration favors the pyramidal coordination. The t_{2g} degeneracy is lifted in this coordination yielding the stabilized $3d_{xy}$ and destabilized degenerate $3d_{yz}$ and $3d_{zx}$ orbitals, as provided in Figure 1 (a). The single *d* electron therefore occupies the $3d_{xy}$ orbital and the $3d^1$ electronic configuration results in enhancement of the pyramidal distortion owing to the Jahn-Teller effect.[8, 30, 31] The $3d_{xy}$ electron is localized due to strong coulomb repulsion. $PbVO_3$ therefore exhibits semiconducting behavior (Mott-insulator). Because of the $3d_{xy}$ orbital ordering, two-dimensional magnetism with competing nearest and next nearest neighbor interactions, which can be reproduced by a S = 1/2 square lattice model, was observed.[30, 32, 33] $PbVO_3$ undergoes a tetragonal-to-cubic phase transition at high pressure of 3 GPa at room temperature.[34-36] This structural transition is accompanied by an insulator-to-metal transition because the single *d*-electron occupies the triply degenerated t_{2g} orbital in the cubic phase.[36] However, the giant c/a ratio prohibits the temperature induced transition to the paraelectric phase and the polarization reversal by electric field.

In this study, $Na_{1/2}Bi_{1/2}VO_3$ and $K_{1/2}Bi_{1/2}VO_3$ are synthesized as means to reduce the c/a ratio of $PbVO_3$. The materials design, i.e., replacement of Pb^{2+} with $(Na_{1/2}Bi_{1/2})^{2+}$ and $(K_{1/2}Bi_{1/2})^{2+}$, whereby the effect of $6s^2$ lone pair is weakened, worked well. Similarly, replacement of Pb^{2+} in $PbTiO_3$ lead to lead-free $Na_{1/2}Bi_{1/2}TiO_3$ (rhombohedral *R3c* or monoclinic *Cc* at RT, tetragonal *P4bm* above 528 K) and $K_{1/2}Bi_{1/2}TiO_3$ (tetragonal *P4mm*, c/a = 1.01-1.02).[37-43] Both the spontaneous polarization in $Na_{1/2}Bi_{1/2}TiO_3$ and $K_{1/2}Bi_{1/2}TiO_3$ are smaller than that in $PbTiO_3$ because the stereo-chemically active Bi^{3+} occupies only half of the *A*-site. Since the replacement of $Ti^{4+}(3d^0)$ with $V^{4+}(3d^1)$ in $PbTiO_3$ results in the enhancement of the tetragonal distortion, a "moderate" tetragonal distortion is realized in $Na_{1/2}Bi_{1/2}VO_3$ and $K_{1/2}Bi_{1/2}VO_3$ perovskites. The valence states are $Na^+(K^+)_{1/2}Bi^{3+}{}_{1/2}V^{4+}O_3$. Semiconducting behaviors were observed for both compounds. Stress-strain measurements revealed existence of ferroelastic-domain switching. Magnetic measurements indicated that these compounds had the $3d_{xy}$ orbital ordering as in $PbVO_3$. Our experimental results on valence, electronic and magnetic structure have been substantiated by theoretical calculations within the framework of density functional theory (DFT).

2. METHODS SECTION

Experimental. $Na_{1/2}Bi_{1/2}VO_3$ and $K_{1/2}Bi_{1/2}VO_3$ were prepared by treating a mixture of Bi_2O_3, $NaVO_3$, KVO_3, and V_2O_3 at 6 GPa and 1473 K for 30 min in a cubic anvil cell-type high-pressure apparatus. $NaVO_3$ and KVO_3 were prepared by heating mixtures of Na_2CO_3, K_2CO_3, and V_2O_5 at 823 K and 733 K, respectively, for 24 hours with intermediate grinding. Synthesized $NaVO_3$ and KVO_3 were checked by powder XRD. Synchrotron X-ray diffraction (SXRD) data for $Na_{1/2}Bi_{1/2}VO_3$ and $K_{1/2}Bi_{1/2}VO_3$ under ambient conditions were collected with the large Debye–Scherrer camera installed on the BL02B2 beamline of SPring-8 (wavelength of 0.420172(1) Å).[44] The diffraction data were analyzed with the Rietveld method using the RIETAN-FP program.[45, 46] Relative densities of the samples were about 95% of the theoretical density. The temperature dependence of the magnetic susceptibility and magnetic field dependence of magnetization of $Na_{1/2}Bi_{1/2}VO_3$ and $K_{1/2}Bi_{1/2}VO_3$ were measured with a SQUID magnetometer (Quantum Design, MPMS). The heat capacity measurements were performed using a physical property measurement system (PPMS, Quantum Design). The temperature dependence of the electrical resistivity of the bulk samples was obtained by means of two-probe method ($K_{1/2}Bi_{1/2}VO_3$) and four-probe method ($Na_{1/2}Bi_{1/2}VO_3$) using a data logger (34972A, Agilent). Electrical resistivity under high pressure up to 6 GPa was quantified using the same data logger and cubic anvil cell-type high-pressure apparatus. Molybdenum sheets were used as the electrodes. *P-E* curves were determined using the Ferroelectric testing system (FCE, TOYO) at 10 K. Au wires were attached with Ag paste on surfaces of the bulk samples. Ferroelastic measurements were performed using a screw-driven load frame (Z010, Zwick GmbH & Co. KG, Ulm, Germany). Cylindrical samples of 2.96 mm in diameter and 2.29 mm in thickness were used. A pre-stress of -5 MPa was applied on the sample to assure a smooth contact. Compressive mechanical stresses up to -150 MPa were applied on unpoled $K_{1/2}Bi_{1/2}VO_3$ with a rate of 1 MPa/s at room temperature. Strain was monitored using a linear variable differential transformer (LVDT) with an estimated error of ~5%, located near the sample.

Theoretical The theoretical calculations have been performed using DFT in the plane-wave basis and in the linear muffin-tin orbital (LMTO) basis, as implemented in the Vienna ab-initio simulation package (VASP)[47, 48] and in the Stuttgart code[49] respectively. For the plane-wave calculations, following pseudo-potential configurations were used, Bi: [core]$5d^{10}6s^26p^3$; Na:[core]$2p^63s^1$; K: [core]$3s^23p^64s^1$; V:[core]$3p^63d^34s^2$; O: [core]$2s^22p^4$. The exchange-correlation density functional was chosen to be generalized gradient approximation (GGA) in the Perdew-Burke-Ernzerhof (PBE)[50] formalism. The missing electron-electron correction effect beyond GGA at the transition metal V site was incorporated by including an onsite Hubbard U (U = 4 eV) and Hund's coupling (J_H = 0.7 eV) within GGA+U formalism.[51] Change in U value by 1-2 eV was found to keep the qualitative results intact. Since it is known that Perdew-Burke-Ernzerhof for solids (PBEsol)[52] reproduces

the experimental lattice parameters better than GGA, especially for ferroelectric compounds, optimization of different structural models were carried out with PBEsol. The plane wave cut-off energy was chosen to be 600 eV. For the Brillouin-zone integration, an 8 × 8 × 8 k-mesh was used for the 2 × 2 × 2 supercells of $Na_{1/2}Bi_{1/2}VO_3$ and $K_{1/2}Bi_{1/2}VO_3$ with 40 atoms in the cell. In addition to all orbital calculations, we have also studied the low energy model Hamiltonian as derived in the N-th order muffin-tin orbital (NMTO) downfolding method.[53, 54]

3. RESULTS AND DISCUSSION

Crystal Structure of $Na_{1/2}Bi_{1/2}VO_3$ and $K_{1/2}Bi_{1/2}VO_3$. Perovskite $Na_{1/2}Bi_{1/2}VO_3$ and $K_{1/2}Bi_{1/2}VO_3$ were successfully synthesized using the high pressure technique. Figures 1 (b) and (c) display the obtained SXRD patterns for $Na_{1/2}Bi_{1/2}VO_3$ and $K_{1/2}Bi_{1/2}VO_3$, which were indexed using the space group *P4mm* in tetragonal symmetry, the same as $PbTiO_3$. The absence of supercell reflections preclude the existence of long-range order of the bismuth and alkali metal ions without making a statement on local order.[40] $Na_{1/2}Bi_{1/2}VO_3$ and $K_{1/2}Bi_{1/2}VO_3$ polycrystalline samples contained a small amount of nonmagnetic impurities, including Bi_2O_3, $NaVO_3$, and KVO_3. Anisotropic line broadening, commonly reported for ferroelectric compounds, was observed.[21, 55-58] The broadening was described by Stephen's phenomenological model in the fitting.[59] The refined occupation factors of bismuth and alkali metals were close to 0.5. Table 1 provides the refined structural parameters with reliability factors for $Na_{1/2}Bi_{1/2}VO_3$ and $K_{1/2}Bi_{1/2}VO_3$. Small reliability factors and reasonable atomic displacement factors *U* were obtained. The determined crystal structures are presented in Figure 1 (d) and (e).

The V-O bond lengths and the bond valence sums (BVSs)[60-63] of each compound are summarized in Table 2. The average bond valence parameters for Bi^{3+} and Na^+ or K^+ were used for the calculation. The BVSs for the *A*-site and *B*-site were approximately 2+ and 4+, respectively. Considering the monovalent nature of sodium and potassium ions, the valence state of these compounds should be $Na^+_{1/2}Bi^{3+}_{1/2}V^{4+}O^{2-}_3$ and $K^+_{1/2}Bi^{3+}_{1/2}V^{4+}O^{2-}_3$.

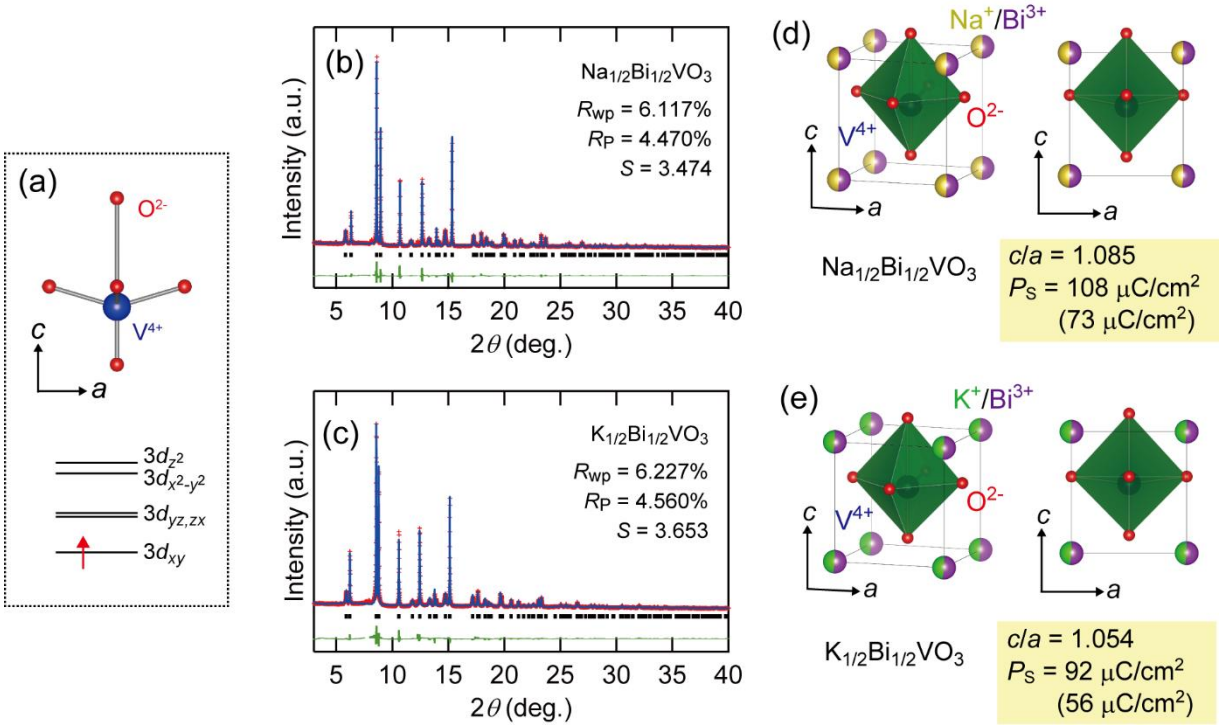

Figure 1 (a) 3*d* energy levels of V^{4+} in a pyramidal coordination environment. Observed (red points), calculated (blue line), and difference (green line) SXRD patterns of (b) $Na_{1/2}Bi_{1/2}VO_3$ and (c) $K_{1/2}Bi_{1/2}VO_3$ at room temperature. The tick marks correspond to the position of Bragg reflections of the *P4mm* tetragonal phase. The larger views of the plots are presented in Figure S1. Crystal structure of (d) $Na_{1/2}Bi_{1/2}VO_3$ and (e) $K_{1/2}Bi_{1/2}VO_3$. The values of spontaneous polarization (P_S) were calculated using Berry phase formalism and point charge model (noted in parentheses).

Table 1 Refined structural parameters and reliability factors of $Na_{1/2}Bi_{1/2}VO_3$ and $K_{1/2}Bi_{1/2}VO_3$

		$Na_{1/2}Bi_{1/2}VO_3$[a]	$K_{1/2}Bi_{1/2}VO_3$[a]
Na/K	*z*	0	0
	U (Å²)	0.0218(3)	0.0312(4)
	g	0.492(2)	0.484(2)
Bi	*z*	0	0
	U (Å²)	0.0218(3)	0.0312(4)
	g	0.508(2)	0.516(2)
V	*z*	0.5687(7)	0.5746(7)
	U (Å²)	0.0134(6)	0.0124(7)
O(1)	*z*	0.1571(16)	0.1488(20)
	U (Å²)	0.0145(13)	0.0212(16)
O(2)	*z*	0.6565(11)	0.6309(14)
	U (Å²)	0.0145(13)	0.0212(16)
a	(Å)	3.81047(5)	3.87736(6)
c	(Å)	4.13336(11)	4.08899(13)
c*/*a		1.08474(2)	1.05458(2)
V	(Å³)	60.0151(20)	61.4735(25)
ρ_{calc}	(g/cm³)	5.986	6.098
R_{wp}	(%)	6.117	6.227
R_p	(%)	4.470	4.560
S		3.474	3.653

[a]Space group: *P4mm* (No. 99), *Z* = 1; The temperature factors of the *A*-site cations and of the O(1) and O(2), respectively, were assumed to be the same.

Table 2 *A*-O and V-O bond lengths and BVSs for $Na_{1/2}Bi_{1/2}VO_3$ and $K_{1/2}Bi_{1/2}VO_3$

	$Na_{1/2}Bi_{1/2}VO_3$	$K_{1/2}Bi_{1/2}VO_3$
***A*-O(1) (Å)**	2.772(2)	2.808(2)
***A*-O(2) (Å)**	2.376(3)	2.457(4)
***A*-O(2)' (Å)**	3.316(4)	3.227(5)
BVS[a] (*A*-site)	1.803	2.324
V-O(1) (Å)	1.701(8)	1.741(9)
V-O(1)' (Å)	2.432(8)	2.348(9)
V-O(2) (Å)	1.940(1)	1.952(1)
BVS[a] (*B*-site)	4.051	3.879

[a]$V_i = \Sigma_j S_{ij}$, $S_{ij} = \exp\{(r_o - r_{ij})/0.37\}$. Values calculated using r_o = 1.784 for V^{4+}, r_o = 2.094 for Bi^{3+}, 1.803 for Na^+ and 2.113 for K^+. Values of r_o were taken as the average of each ion in $Na_{1/2}Bi_{1/2}VO_3$ (1.9508) and $K_{1/2}Bi_{1/2}VO_3$ (2.1032).

The *c*/*a* ratio was 1.085 and 1.054 for $Na_{1/2}Bi_{1/2}VO_3$ and $K_{1/2}Bi_{1/2}VO_3$, respectively. On the basis of a Berry phase using the method developed by King-Smith and Vanderbilt,[64, 65] the spontaneous polarizations (P_S) were calculated. The computed polarization is expected to provide better theoretical estimate compared to point charge model which does not include the electronic contribution. The polarization computed using the Berry phase formalism gave rise to values of 108 μC/cm² for $Na_{1/2}Bi_{1/2}VO_3$, and 92 μC/cm² for $K_{1/2}Bi_{1/2}VO_3$, in comparison to point charge estimates of 73 μC/cm² and 56 μC/cm², respectively. These values are comparable to those of $PbTiO_3$ with *c*/*a* = 1.065, approximately 90-100 μC/cm² by Berry phase approach,[66-68] and 59 μC/cm² by the point charge model.[7] Interestingly, the spontaneous polarizations are roughly proportional to the *c*/*a* ratios, as displayed in Figure 2. $Na_{1/2}Bi_{1/2}VO_3$ has grater *c*/*a* ratio than $K_{1/2}Bi_{1/2}VO_3$, while the structural optimization calculation find the *c*/*a* ratios to be roughly comparable, the details being dependent on the local structure model (see Table S1).

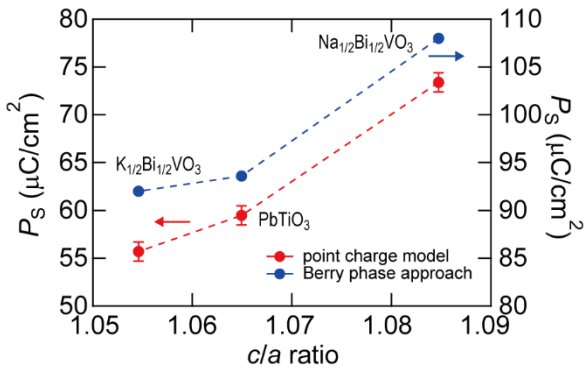

Figure 2 Spontaneous polarization as a function of c/a ratio. The value of P_S for $PbTiO_3$ by Berry phase approach was cited by reference 67.

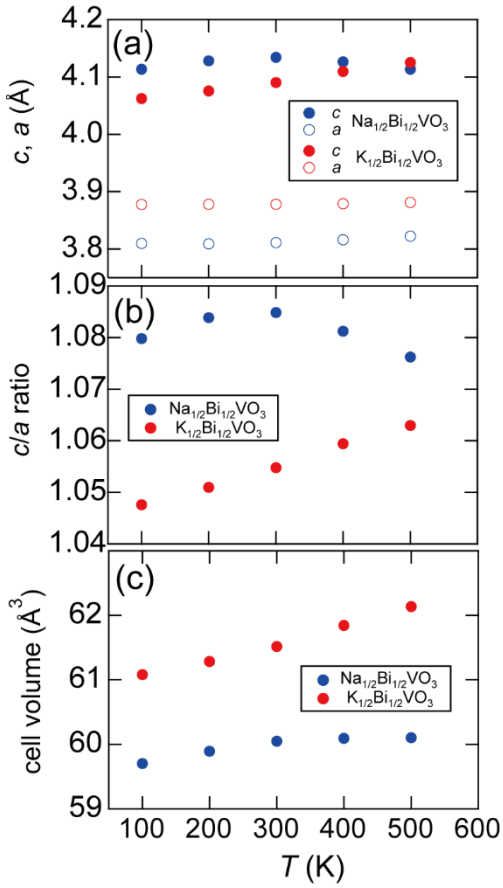

Figure 3 Temperature dependence of (a) lattice parameters c and a, (b) c/a ratios, and (c) cell volumes in $Na_{1/2}Bi_{1/2}VO_3$ and $K_{1/2}Bi_{1/2}VO_3$.

Temperature-dependent SXRD up to 900 K features the transition to the paraelectric phase. However, as depicted in Figure S1, the tetragonal phase was preserved up to the decomposition temperature of 600 K for both $Na_{1/2}Bi_{1/2}VO_3$ and $K_{1/2}Bi_{1/2}VO_3$. The decomposed products were $Bi_4V_3O_{12}$, Bi_2VO_5, Bi_2O_3, $Na_2V_6O_{16}$, and Na_3VO_4 for $Na_{1/2}Bi_{1/2}VO_3$ and $Bi_4V_3O_{12}$, Bi_2O_3, and $K_3V_3O_8$ for $K_{1/2}Bi_{1/2}VO_3$. Figure 3 reveals the temperature dependence of lattice parameters, c/a ratios, and unit cell volumes. The c/a ratio decreased above 300 K in $Na_{1/2}Bi_{1/2}VO_3$, while that of $K_{1/2}Bi_{1/2}VO_3$ kept increasing up to 500 K. The cause for the different c/a ratio change at high temperatures is unclear at the present stage.

Evidence of electron localization in the $3d_{xy}$ orbital of tetragonal $Na_{1/2}Bi_{1/2}VO_3$ and $K_{1/2}Bi_{1/2}VO_3$. Figure 4 (a) and (b) depict the temperature dependence of zero field cooling (ZFC) and field cooling (FC) magnetic susceptibility (M/H) data down to 2 K, measured in a magnetic field of 0.1 T. FC data between 200 and 300 K were fitted to the Curie-Weiss law with temperature independent term. The effective magnetic moments, $\mu_{eff} = g(S(S+1))^{1/2}\mu_B$, were 1.64 μ_B (C = 0.338) and 1.70 μ_B (C = 0.361) in $Na_{1/2}Bi_{1/2}VO_3$ and $K_{1/2}Bi_{1/2}VO_3$, respectively. These values are close to the value of 1.73 μ_B expected for V^{4+} (S=1/2) with g = 2 indicating that the systems are localized antiferromagnets, owing to the ordering of the $3d_{xy}$ orbital. Curie-Weiss temperatures (θ_{CW}) were -205 K in $Na_{1/2}Bi_{1/2}VO_3$ and -187 K in $K_{1/2}Bi_{1/2}VO_3$. Deviations between ZFC and FC data suggesting spin glass freezing were observed at 3 and 6 K, less than 1/30 of θ_{CW}, for $Na_{1/2}Bi_{1/2}VO_3$ and $K_{1/2}Bi_{1/2}VO_3$, respectively, as highlighted in insets of Figures 4(a) and (b). Accordingly, no λ-like peak indicating long-range ordering was observed in specific heat data (see Figure S2). These reflect the geometrical frustration stemming from competing nearest and next-nearest in-plane antiferromagnetic interactions as discussed later.

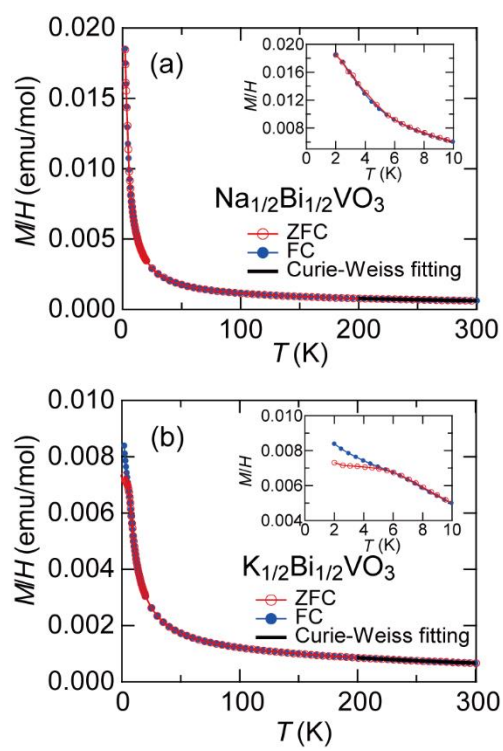

Figure 4 Temperature dependence of magnetic susceptibility of (a) $Na_{1/2}Bi_{1/2}VO_3$ and (b) $K_{1/2}Bi_{1/2}VO_3$. The black

lines between 200 and 300 K (FC) feature the results of fitting to the Curie-Weiss law with a temperature independent term χ_0 : $M/H = C/(T-\theta_{CW}) + \chi_0$, where the term C is the Curie constant and θ_{CW} is the Curie-Weiss temperature. The inset provides a magnified view of M/H-T plot below 20 K. The dotted lines depict the extrapolation of the linear region.

Accordingly, semiconductive behavior was observed in the DC electrical resistivity of $Na_{1/2}Bi_{1/2}VO_3$ and $K_{1/2}Bi_{1/2}VO_3$, as provided in Figure 5 (a) and (b). The resistivity below 150 K for $Na_{1/2}Bi_{1/2}VO_3$ and 250 K for $K_{1/2}Bi_{1/2}VO_3$ reached the upper limit of our experimental setup. At room temperature the resistivity of $K_{1/2}Bi_{1/2}VO_3$ was ~10^4 times higher than that of $Na_{1/2}Bi_{1/2}VO_3$. The absence of metallic conduction in these compounds indicates that the pyramidal distortion of the V-O octahedron lifts the t_{2g} degeneracy, as in $PbVO_3$. The Curie-Weiss like paramagnetism also supports the localized single electron in the $3d_{xy}$ orbital. These results indicate the Jahn-Teller effect in the V^{4+}-O octahedron.

Pressure dependence of DC electrical resistivity was obtained to confirm that the insulator-to-metal transition is accompanied by a paraelectric transition. The resistivity decreased sharply around 2 GPa in $Na_{1/2}Bi_{1/2}VO_3$ (Figure 5 (c)). This is similar to the pressure-induced insulator-to-metal transition in $PbVO_3$. The transition pressure of ~2 GPa in $Na_{1/2}Bi_{1/2}VO_3$ is lower than that of ~3 GPa in $PbVO_3$ because of the smaller c/a ratio and spontaneous polarization. In contrast, $K_{1/2}Bi_{1/2}VO_3$ did not reveal a prominent transition below 6 GPa. A second-order like tetragonal-to-cubic transition at high pressure of 11.2 GPa was reported in $PbTiO_3$ at room temperature,[69] while $PbVO_3$ reveals a first-order tetragonal-to-cubic transition at 3 GPa.[34, 35, 70] Because $K_{1/2}Bi_{1/2}VO_3$ and $PbTiO_3$ have closer c/a ratios and spontaneous polarizations than $Na_{1/2}Bi_{1/2}VO_3$ and $PbTiO_3$, the transition in $K_{1/2}Bi_{1/2}VO_3$ might have a second order-like nature, as in $PbTiO_3$. Further studies, including XRD measurement at high pressure are necessary to clarify the origin of this behavior.

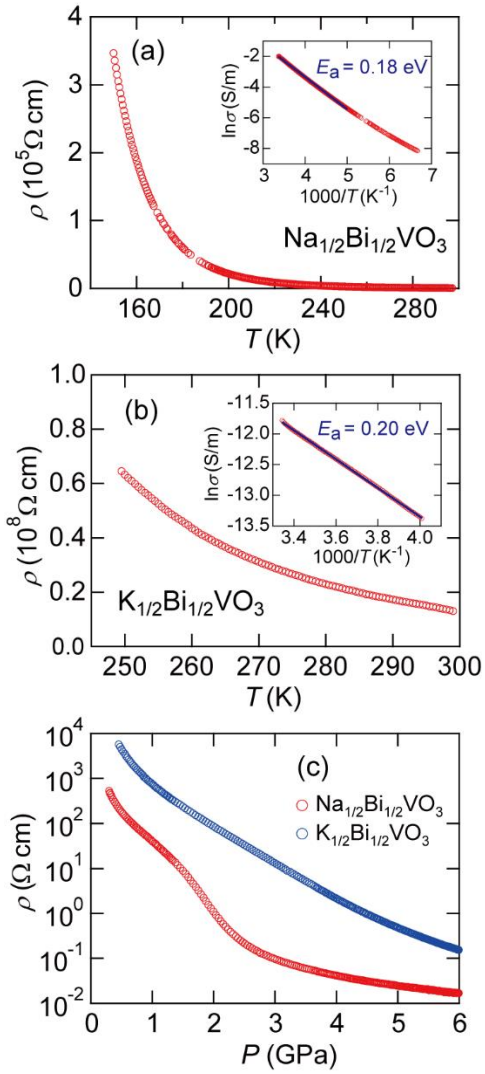

Figure 5 Temperature dependence of electrical resistivity in (a) $Na_{1/2}Bi_{1/2}VO_3$ and (b) $K_{1/2}Bi_{1/2}VO_3$. (c) Pressure dependence of electrical resistivity up to 6 GPa.

DFT results. For the theoretical calculations, we have constructed 2 × 2 × 2 supercells of $Na_{1/2}Bi_{1/2}VO_3$ and $K_{1/2}Bi_{1/2}VO_3$ with half of the A sites populated by Bi atoms and another half by Na/K atoms. In order to take into account the ordering tendency and the effect of local structure, following the discussion in references [71-73], we considered six distinct possible arrangements of Na/K and Bi atoms. The details of the calculations can be found in supporting information. The spin-polarized density of states (DOS) for $Na_{1/2}Bi_{1/2}VO_3$ and $K_{1/2}Bi_{1/2}VO_3$ in their minimum energy local structure of A-site cation arrangement are displayed in Figure 6 (a) and (b), respectively. The DOS features the expected insulating behavior in agreement with the experimental DC electric resistivity measurement. The DOS has been projected onto the Bi-s and p, V-d, and O-p states. The empty p states and filled s states of Bi confirm its 3+ charge state. The calculated magnetic moment at V site turned out to be ~0.99 μ_B, assuring a valence state of 4+ with d^1 electronic configuration, in agreement with the

conclusion drawn from the Curie-Weiss fitting. This puts the alkali ion and oxygen in usual 1+ and 2- charge state, respectively. The splitting of V-*d* states in the distorted pyramidal coordination offered by oxygens, is well reflected in the DOS (as marked in the figures). The up channel of d_{xy} is the only filled orbital, contributing to the magnetic properties of these systems, the other V-*d* states being completely empty in both spin channels. The insets in the figures depict the crystal field splitting at the V site, as given by NMTO-downfolding construction of V-*d* only Hamiltonian in two compounds. As seen, this consists of split d_{xy} energy levels separated by a gap of 0.2-0.4 eV from nearly degenerate d_{xz}/d_{yz} levels, which are further separated by a large energy gap of 1-1.2 eV from d_{x2-y2} and d_{z2} states. The energy splitting between d_{x2-y2} and d_{z2} states is found to be larger for $Na_{1/2}Bi_{1/2}VO_3$ compared to that in $K_{1/2}Bi_{1/2}VO_3$, reflecting the larger tetragonality in the former.

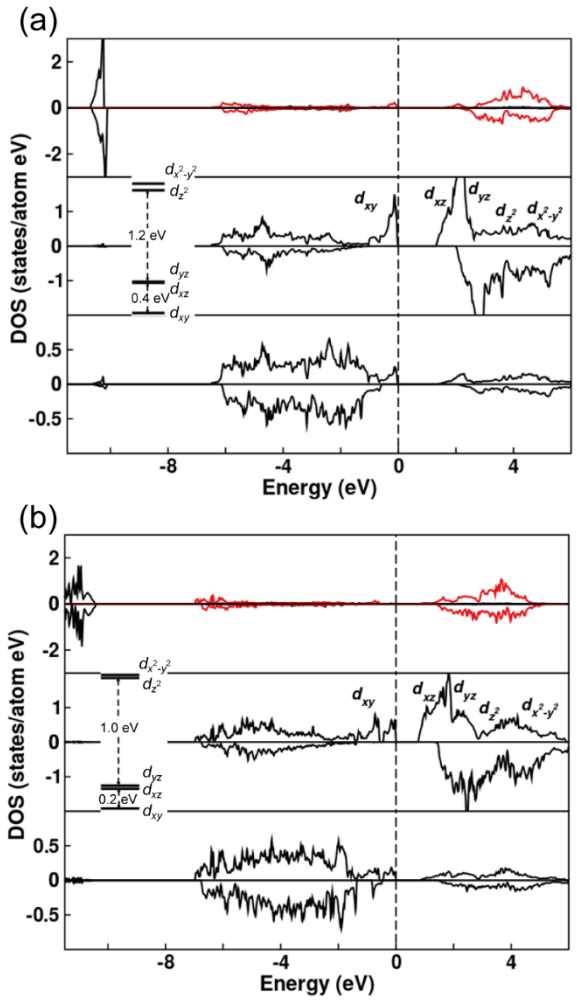

Figure 6 The spin-polarized DOS of (a) $Na_{1/2}Bi_{1/2}VO_3$ and (b) $K_{1/2}Bi_{1/2}VO_3$ projected to various states at the optimized crystal geometry in the lowest energy local structure of *A*-site cation distribution. The Bi (*s* in black, *p* in red), V *d* and O *p* states are featured in top, middle and bottom panels, respectively. The calculated crystal field splitting of the V *d* orbitals are also provided in the inset of the middle panel.

In order to understand the detailed nature of magnetism in $Na_{1/2}Bi_{1/2}VO_3$ and $K_{1/2}Bi_{1/2}VO_3$, we have further carried out calculations considering ferromagnetic (FM) and three antiferromagnetic (AFM) spin configurations: (a) A-type AFM (V spins being coupled ferromagnetically in the *ab*-plane and antiferromagnetically between the planes), (b) C-type AFM (V spins being antiferromagnetically coupled in the *ab*-plane and ferromagnetically between the planes) and (c) G-AFM (V spins being antiferromagnetically connected in-plane as well as out of plane). In both $Na_{1/2}Bi_{1/2}VO_3$ and $K_{1/2}Bi_{1/2}VO_3$, the energy difference between C-type and G-type AFM configuration is found to be small. Similarly the energy difference between FM and A-type AFM configuration is found to be negligible. This suggests a strong antiferromagnetic coupling between V spins in the *ab*-plane, which are weakly coupled in the out of plane direction. This is further substantiated by the estimates of various magnetic exchanges (see Figure 7 for the notation) extracted by mapping the total energy differences of different magnetic configurations to an underlying Heisenberg spin Hamiltonian. From the values listed in Table 3, we find that the in-plane exchanges (J_1 and J_3) to be antiferromagnetic and substantially larger than the out of plane ferromagnetic exchanges (J_1 and J_3). These systems can therefore be regarded as geometrically frustrated S = 1/2 square-lattice antiferromagnets with competing nearest (J_1) and next-nearest (J_3) interactions. An indicative measure of a θ_{CW} trend between the Na and K compounds may be obtained by considering the formula, defined as $\Sigma J_k \cdot Z_k \cdot S_i \cdot S_j / 3k_B$, where the summation over k runs over the dominant magnetic interactions listed in Table 3. Z_k is the number of neighbors for k-th magnetic interaction, and S_i and S_j are the spin values (S = 1/2) of the magnetic V sites at i and j defining the magnetic interactions. We estimate the θ_{CW} of the $Na_{1/2}Bi_{1/2}VO_3$ to be -268 K and the $K_{1/2}Bi_{1/2}VO_3$ to be -220 K, in good agreement with experimental values of -205 K and -187 K respectively.

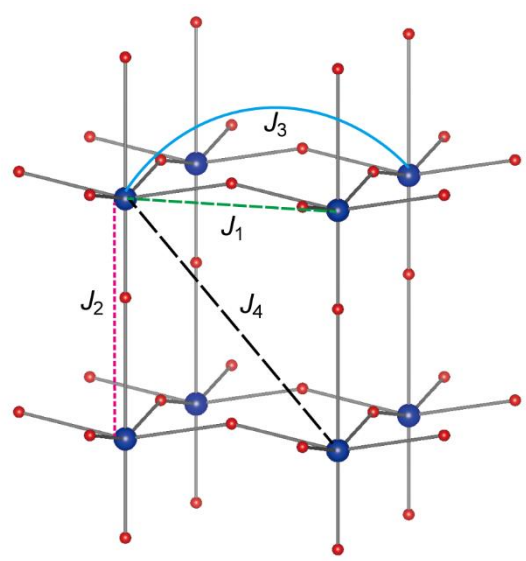

Figure 7 The magnetic exchange paths between V spins in $Na_{1/2}Bi_{1/2}VO_3$ ($K_{1/2}Bi_{1/2}VO_3$). The J_1 and J_3 are in-plane interactions, while the J_2 and J_4 are out of plane interactions.

Table 3 Computed values of the relevant magnetic coupling constants for $Na_{1/2}Bi_{1/2}VO_3$ and $K_{1/2}Bi_{1/2}VO_3$. Positive values of *J* signify antiferromagnetic coupling while negative values signify ferromagnetic coupling. The exchange pathways are illustrated in Figure 7.

	$Na_{1/2}Bi_{1/2}VO_3$	$K_{1/2}Bi_{1/2}VO_3$
J_1	19.50	16.15
J_2	−0.65	−0.58
J_3	4.13	3.09
J_4	−0.10	−0.05

Ferroelastic domain switching and possibility of ferroelectric switching in $K_{1/2}Bi_{1/2}VO_3$ and $Na_{1/2}Bi_{1/2}VO_3$. Finally, we discuss the possibility of ferroelectric domain switching. The stress-strain measurement of the $K_{1/2}Bi_{1/2}VO_3$ polycrystalline sample is depicted in Figure 8. The curves exhibit non-linear behavior, characteristic for ferroelastic perovskite materials.[74] The remanent strain increased up to -0.164% upon increasing the maximum stress to -150 MPa. The ferroelastic behavior is attributed to the switching of 90° ferroelectric/ferroelastic domains. The load was limited to -150 MPa to prevent the breaking of the sample. The coercive stress could not be unambiguously determined. Considering the large *c*/*a* ratio of 1.054, the coercive stress is expected to be higher than the maximum stress applied during this measurement. In addition, *P*-*E* measurements were performed at 10 K on a $K_{1/2}Bi_{1/2}VO_3$ polycrystalline sample. No ferroelectric hysteresis loop could be observed up to a field of 200 kV/cm, as provided in Figure S7. A second phase may hinder domain switching and effectively lead to electromechanical hardening. Applying higher electric fields should be necessary to observe ferroelectric switching in $K_{1/2}Bi_{1/2}VO_3$. This observation is in agreement with calculated DFT energy curves as a function of ferroelectric polarization, which reveal that switching may possibly happen in these compounds, but upon application of rather large electric field (see Figure S6). Ferroelectric and ferroelastic measurements were performed only for $K_{1/2}Bi_{1/2}VO_3$ polycrystalline samples, since $Na_{1/2}Bi_{1/2}VO_3$ was too brittle to prepare the required thin disc and cylinder sample geometries. However, due to the chemical and structural similarities, ferroelastic behavior is also expected in $Na_{1/2}Bi_{1/2}VO_3$.

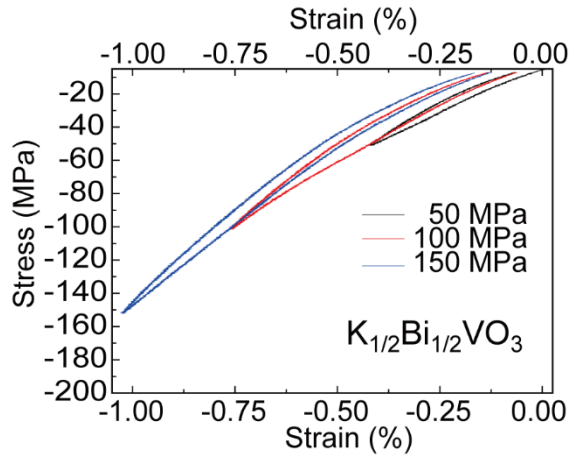

Figure 8 Stress-strain curves obtained during repeated loading with increasing amplitude of a $K_{1/2}Bi_{1/2}VO_3$ polycrystalline sample. The sample dimensions were 2.96 mm in diameter and 2.29 mm in thickness.

4. CONCLUSION

New lead-free tetragonal perovskites $Na_{1/2}Bi_{1/2}VO_3$ and $K_{1/2}Bi_{1/2}VO_3$ were synthesized at high pressure and high temperature condition of 6 GPa and 1473 K. Both compounds exhibit a *c*/*a* ratio and P_S comparable to the lead-based ferroelectric $PbTiO_3$: *c*/*a* = 1.085 and P_S = 108 μC/cm² (73 μC/cm² by point charge model) for $Na_{1/2}Bi_{1/2}VO_3$ and *c*/*a* = 1.054 and P_S = 92 μC/cm² (56 μC/cm² by point charge model) for $K_{1/2}Bi_{1/2}VO_3$. Magnetic and electric properties indicated the lifted t_{2g} degeneracy and $3d_{xy}$ orbital ordering caused by a Jahn-Teller effect. The experimental results were further corroborated in terms of first-principles DFT calculations which confirmed the valence of V, estimated the crystal field splitting and derived the detailed electronic and magnetic structure. Ferroelastic behavior was observed by means of stress-strain measurement on $K_{1/2}Bi_{1/2}VO_3$ polycrystalline sample, indicating the ferroelectric/ferroelastic nature of the sample. The present results provide a guideline to design new lead-free ferroelectric and piezoelectric materials based on the idea of cooperation of an optimized *A*-site and the Jahn-Teller active *B*-site cation possessing $3d^1$ (or $3d^6$ electron) configurations. $Na_{1/2}Bi_{1/2}VO_3$ and $K_{1/2}Bi_{1/2}VO_3$ can be used as tetragonal end members for the formation of new solid solutions with rhombohedral compositions, which are expected to exhibit morphotropic phase boundaries and thus enhanced dielectric and piezoelectric properties.

ASSOCIATED CONTENT

Supporting Information

The Supporting Information is available free of charge on the ACS Publications website at

Larger views of obtained and calculated SXRD pattern, temperature change XRD data, temperature dependence of inverse magnetic susceptibility, magnetization curves, temperature dependence of heat capacity, structural models and the corresponding energies, variation of energy as a function of ferroelectric polarization, structural information and calculated band gap of the structural models, electric field dependence of spontaneous polarization (*P-E* measurement)

AUTHOR INFORMATION

Corresponding Authors

*hajime.yamamoto.a2@tohoku.ac.jp
*mazuma@msl.titech.ac.jp

Present Addresses

°Institute of Multidisciplinary Research for Advanced Materials, Tohoku University, Katahira2-1-1, Aoba-ku, Sendai 980-8577, Japan

Author Contributions

The manuscript was written through contributions of all authors. / All authors have given approval to the final version of the manuscript.

ACKNOWLEDGMENT

This work was partially supported by the Grant-in-Aid for Scientific Research, 16H02393, from the Japan Society for the Promotion of Science (JSPS) and by the Kanagawa Institute of Industrial Science and Technology. The synchrotron-radiation experiments were performed at SPring-8 with the approval of the Japan Synchrotron Radiation Research Institute (2017B1697). SP is indebted for support provided by a fellowship of the Alexander-von-Humboldt foundation. T.S-D and A.P acknowledge help of Subhadeep Bandyopadhyay in some of the DFT calculations.

REFERENCES

1. Jaffe, B.; Roth, R. S.; Marzullo, S., Properties of piezoelectric ceramics in the solid-solution series lead-titanate-lead zirconate-lead oxide-tin oxide and lead titanate-lead hafnate. *J. Res. Natl. Bur. Stand.* **1955,** *55*, 239-254.
2. Guo, R.; Cross, L. E.; Park, S. E.; Noheda, B.; Cox, D. E.; Shirane, G., Origin of the high piezoelectric response in $PbZr_{1-x}Ti_xO_3$. *Phys. Rev. Lett.* **2000,** *84*, 5423-5426.
3. Noheda, B.; Cox, D. E.; Shirane, G.; Guo, R.; Jones, B.; Cross, L. E., Stability of the monoclinic phase in the ferroelectric perovskite $PbZr_{1-x}Ti_xO_3$. *Phys. Rev. B* **2001,** *63*, 014103.
4. Shirane, G.; Hoshino, S.; Suzuki, K., X-ray study of the phase transition in lead titanate. *Phys. Rev.* **1950,** *80*, 1105-1106.
5. Shirane, G.; Hoshino, S., On the phase transition in lead titanate. *J. Phys. Soc. Jpn.* **1951,** *6*, 265-270.
6. Cohen, R. E., Origin of ferroelectricity in perovskite oxides. *Nature* **1992,** *358*, 136-138.
7. Kuroiwa, Y.; Aoyagi, S.; Sawada, A.; Harada, J.; Nishibori, E.; Takata, M.; Sakata, M., Evidence for Pb-O covalency in tetragonal $PbTiO_3$. *Phys. Rev. Lett.* **2001,** *87*, 217601.
8. Kunz, M.; Brown, I. D., Out-of-center distortions around octahedrally coordinated d^0 transition-metals. *J. Solid State Chem.* **1995,** *115*, 395-406.
9. Shrout, T. R.; Zhang, S. J., Lead-free piezoelectric ceramics: Alternatives for PZT? *J. Electroceram.* **2007,** *19*, 113-126.
10. Rödel, J.; Jo, W.; Seifert, K. T. P.; Anton, E. M.; Granzow, T.; Damjanovic, D., Perspective on the Development of Lead-free Piezoceramics. *J. Am. Ceram. Soc.* **2009,** *92*, 1153-1177.
11. Wang, X. P.; Wu, J. G.; Xiao, D. Q.; Zhu, J. G.; Cheng, X. J.; Zheng, T.; Zhang, B. Y.; Lou, X. J.; Wang, X. J., Giant Piezoelectricity in Potassium-Sodium Niobate Lead-Free Ceramics. *J. Am. Chem. Soc.* **2014,** *136*, 2905-2910.
12. Takenaka, T.; Maruyama, K.; Sakata, K., $(Bi_{1/2}Na_{1/2})TiO_3$-$BaTiO_3$ system for lead-free piezoelectric ceramics. *Jpn. J. Appl. Phys., Part 1* **1991,** *30*, 2236-2239.
13. Acosta, M.; Novak, N.; Rojas, V.; Patel, S.; Vaish, R.; Koruza, J.; Rossetti, G. A.; Rödel, J., $BaTiO_3$-based piezoelectrics: Fundamentals, current status, and perspectives. *Appl. Phys. Rev.* **2017,** *4*, 041305.
14. Saito, Y.; Takao, H.; Tani, T.; Nonoyama, T.; Takatori, K.; Homma, T.; Nagaya, T.; Nakamura, M., Lead-free piezoceramics. *Nature* **2004,** *432*, 84-87.
15. Liu, W. F.; Ren, X. B., Large Piezoelectric Effect in Pb-Free Ceramics. *Phys. Rev. Lett.* **2009,** *103*, 257602.
16. Lee, M. H.; Kim, D. J.; Park, J. S.; Kim, S. W.; Song, T. K.; Kim, M. H.; Kim, W. J.; Do, D.; Jeong, I. K., High-Performance Lead-Free Piezoceramics with High Curie Temperatures. *Adv. Mater.* **2015,** *27*, 6976-6982.
17. Yashima, M.; Omoto, K.; Chen, J.; Kato, H.; Xing, X. R., Evidence for (Bi,Pb)-O Covalency in the High T_C Ferroelectric $PbTiO_3$-$BiFeO_3$ with Large Tetragonality. *Chem. Mater.* **2011,** *23*, 3135-3137.
18. Belik, A. A.; Iikubo, S.; Kodama, K.; Igawa, N.; Shamoto, S.; Niitaka, S.; Azuma, M.; Shimakawa, Y.; Takano, M.; Izumi, F.; Takayama-Muromachi, E., Neutron powder diffraction study on the crystal and magnetic structures of $BiCoO_3$. *Chem. Mater.* **2006,** *18*, 798-803.
19. Uratani, Y.; Shishidou, T.; Ishii, F.; Oguchi, T., First-principles predictions of giant electric polarization. *Jpn. J. Appl. Phys., Part 1* **2005,** *44*, 7130-7133.
20. Suchomel, M. R.; Fogg, A. M.; Allix, M.; Niu, H. J.; Claridge, J. B.; Rosseinsky, M. J., Bi_2ZnTiO_6: A lead-free closed-shell polar perovskite with a calculated ionic polarization of 150 $\mu C\ cm^{-2}$. *Chem. Mater.* **2006,** *18*, 4987-4989.
21. Yu, R.; Hojo, H.; Oka, K.; Watanuki, T.; Machida, A.; Shimizu, K.; Nakano, K.; Azuma, M., New $PbTiO_3$-Type Giant Tetragonal Compound Bi_2ZnVO_6 and Its Stability under Pressure. *Chem. Mater.* **2015,** *27*, 2012-2017.
22. Budimir, M.; Danjanovic, D.; Setter, N., Piezoelectric anisotropy - Phase transition relations in perovskite single crystals. *2004 14th IEEE International Symposium on Applications of Ferroelectrics-ISAF-04* **2004**, 110-113.
23. Shimizu, K.; Hojo, H.; Ikuhara, Y.; Azuma, M., Enhanced Piezoelectric Response due to Polarization Rotation in Cobalt-Substituted $BiFeO_3$ Epitaxial Thin Films. *Adv. Mater.* **2016,** *28*, 8639-8644.
24. Cooper, V. R.; Morris, J. R.; Takagi, S.; Singh, D. J., La-Driven Morphotrophic Phase Boundary in the $Bi(Zn_{1/2}Ti_{1/2})O_3$-$La(Zn_{1/2}Ti_{1/2})O_3$-$PbTiO_3$ Solid Solution. *Chem. Mater.* **2012,** *24*,

4477-4482.
25. Pushkarev, A. V.; Olekhnovich, N. M.; Radyush, Y. V., High-Pressure $Bi(Mg_{1-x}Zn_x)_{1/2}Ti_{1/2}O_3$ Perovskite Solid Solutions. *Inorg. Mater.* **2011,** *47*, 1116-1119.
26. Yu, R. Z.; Matsuda, N.; Tominaga, K.; Shimizu, K.; Hojo, H.; Sakai, Y.; Yamamoto, H.; Oka, K.; Azuma, M., High-Temperature Monoclinic *Cc* Phase with Reduced *c*/*a* Ratio in Bi-based Perovskite Compound $Bi_2ZnTi_{1-x}Mn_xO_6$. *Inorg. Chem.* **2016,** *55*, 6124-6129.
27. Oka, K.; Koyama, T.; Ozaaki, T.; Mori, S.; Shimakawa, Y.; Azuma, M., Polarization Rotation in the Monoclinic Perovskite $BiCo_{1-x}Fe_xO_3$. *Angew. Chem., Int. Ed.* **2012,** *51*, 7977-7980.
28. Azuma, M.; Niitaka, S.; Hayashi, N.; Oka, K.; Takano, M.; Funakubo, H.; Shimakawa, Y., Rhombohedral-tetragonal phase boundary with high curie temperature in (1-*x*)$BiCoO_3$-*x*$BiFeO_3$ solid solution. *Jpn. J. Appl. Phys.* **2008,** *47*, 7579-7581.
29. Shpanchenko, R. V.; Chernaya, V. V.; Tsirlin, A. A.; Chizhov, P. S.; Sklovsky, D. E.; Antipov, E. V.; Khlybov, E. P.; Pomjakushin, V.; Balagurov, A. M.; Medvedeva, J. E.; Kaul, E. E.; Geibel, C., Synthesis, structure, and properties of new perovskite $PbVO_3$. *Chem. Mater.* **2004,** *16*, 3267-3273.
30. Oka, K.; Yamada, I.; Azuma, M.; Takeshita, S.; Satoh, K. H.; Koda, A.; Kadono, R.; Takano, M.; Shimakawa, Y., Magnetic ground-state of perovskite $PbVO_3$ with large tetragonal distortion. *Inorg. Chem.* **2008,** *47*, 7355-7359.
31. Korotin, M. A.; Elfimov, I. S.; Anisimov, V. I.; Troyer, M.; Khomskii, D. I., Exchange interactions and magnetic properties of the layered vanadates CaV_2O_5, MgV_2O_5, CaV_3O_7, and CaV_4O_9. *Phys. Rev. Lett.* **1999,** *83*, 1387-1390.
32. Tsirlin, A. A.; Belik, A. A.; Shpanchenko, R. V.; Antipov, E. V.; Takayama-Muromachi, E.; Rosner, H., Frustrated spin-1/2 square lattice in the layered perovskite $PbVO_3$. *Phys. Rev. B* **2008,** *77*, 092402.
33. Okos, A.; Colin, C.; Darie, C.; Raita, O.; Bordet, P.; Pop, A., Structure and magnetic properties of the layered perovskite $PbVO_3$. *J. Alloys Compd.* **2014,** *602*, 265-268.
34. Zhou, W.; Tan, D. Y.; Xiao, W. S.; Song, M. S.; Chen, M.; Xiong, X. L.; Xu, J., Structural properties of $PbVO_3$ perovskites under hydrostatic pressure conditions up to 10.6 GPa. *J. Phys.: Condens. Matter* **2012,** *24*, 435403.
35. Belik, A. A.; Azuma, M.; Saito, T.; Shimakawa, Y.; Takano, M., Crystallographic features and tetragonal phase stability of $PbVO_3$, a new member of $PbTiO_3$ family. *Chem. Mater.* **2005,** *17*, 269-273.
36. Oka, K.; Yamauchi, T.; Kanungo, S.; Shimazu, T.; Oh-ishi, K.; Uwatoko, Y.; Azuma, M.; Saha-Dasgupta, T., Experimental and Theoretical Studies of the Metallic Conductivity in Cubic $PbVO_3$ under High Pressure. *J. Phys. Soc. Jpn.* **2018,** *87*, 024801.
37. Buhrer, C. F., Some properties of bismuth perovskites. *J. Chem. Phys.* **1962,** *36*, 798-803.
38. Jones, G. O.; Kreisel, J.; Thomas, P. A., A structural study of the $(Na_{1-x}K_x)_{0.5}Bi_{0.5}TiO_3$ perovskite series as a function of substitution (x) and temperature. *Powder Diffr.* **2002,** *17*, 301-319.
39. Aksel, E.; Forrester, J. S.; Jones, J. L.; Thomas, P. A.; Page, K.; Suchomel, M. R., Monoclinic crystal structure of polycrystalline $Na_{0.5}Bi_{0.5}TiO_3$. *Appl. Phys. Lett.* **2011,** 98, 152901.
40. Levin, I.; Reaney, I. M., Nano- and Mesoscale Structure of $Na_{1/2}Bi_{1/2}TiO_3$: A TEM Perspective. *Adv. Funct. Mater.* **2012,** 22, 3445-3452.
41. Aksel, E.; Forrester, J. S.; Nino, J. C.; Page, K.; Shoemaker, D. P.; Jones, J. L., Local atomic structure deviation from average structure of $Na_{0.5}Bi_{0.5}TiO_3$: Combined x-ray and neutron total scattering study. *Phys. Rev. B* **2013,** 87, 104113.
42. Singh, A.; Chatterjee, R., Structural and electrical properties of BKT rich $Bi_{0.5}K_{0.5}TiO_3$-$K_{0.5}Na_{0.5}NbO_3$ system. *Aip Adv.* **2013,** *3*, 032129.
43. Wefring, E. T.; Morozov, M. I.; Einarsrud, M. A.; Grande, T., Solid-State Synthesis and Properties of Relaxor (1-*x*)BKT-*x*BNZ Ceramics. *J. Am. Ceram. Soc.* **2014,** *97*, 2928-2935.
44. Kawaguchi, S.; Takemoto, M.; Osaka, K.; Nishibori, E.; Moriyoshi, C.; Kubota, Y.; Kuroiwa, Y.; Sugimoto, K., High-throughput powder diffraction measurement system consisting of multiple MYTHEN detectors at beamline BL02B2 of SPring-8. *Rev. Sci. Instrum.* **2017,** *88*, 085111.
45. Izumi, F.; Momma, K., Three-dimensional visualization in powder diffraction. *Appl. Crystallogr. XX* **2007,** *130*, 15-20.
46. Momma, K.; Izumi, F., VESTA 3 for three-dimensional visualization of crystal, volumetric and morphology data. *J. Appl. Crystallogr.* **2011,** *44*, 1272-1276.
47. Kresse, G.; Furthmuller, J., Efficiency of ab-initio total energy calculations for metals and semiconductors using a plane-wave basis set. *Comput. Mater. Sci.* **1996,** *6*, 15-50.
48. Kresse, G.; Furthmuller, J., Efficient iterative schemes for ab initio total-energy calculations using a plane-wave basis set. *Phys. Rev. B* **1996,** *54*, 11169-11186.
49. Andersen, O. K., Linear methods in band theory. *Phys. Rev. B* **1975,** *12*, 3060-3083.
50. Perdew, J. P.; Burke, K.; Ernzerhof, M., Generalized gradient approximation made simple. *Phys. Rev. Lett.* **1996,** *77*, 3865-3868.
51. Anisimov, V. I.; Aryasetiawan, F.; Lichtenstein, A. I., First-principles calculations of the electronic structure and spectra of strongly correlated systems: The LDA+U method. *J. Phys.: Condens. Matter* **1997,** *9*, 767-808.
52. Perdew, J. P.; Ruzsinszky, A.; Csonka, G. I.; Vydrov, O. A.; Scuseria, G. E.; Constantin, L. A.; Zhou, X. L.; Burke, K., Restoring the Density-Gradient Expansion for Exchange in Solids and Surfaces. *Phys. Rev. Lett.* **2009,** 102, 136406.
53. Andersen, O. K.; Saha-Dasgupta, T., Muffin-tin orbitals of arbitrary order. *Phys. Rev. B* **2000,** *62*, 16219-16222.
54. Andersen, O. K.; Saha-Dasgupta, T.; Ezhov, S., Third-generation muffin-tin orbitals. *Bull. Mater. Sci.* **2003,** *26*, 19-26.
55. Chen, J.; Xing, X. R.; Yu, R. B.; Liu, G. R.; Wu, L.; Chen, X. L., Structural investigations on ferroelectric $Pb_{1-3/2x}La_xTiO_3$ using the x-ray Rietveld method. *J. Mater. Res.* **2004,** *19*, 3614-3619.
56. Grinberg, I.; Suchomel, M. R.; Dmowski, W.; Mason, S. E.; Wu, H.; Davies, P. K.; Rappe, A. M., Structure and polarization in the high T_C ferroelectric $Bi(Zn,Ti)O_3$-$PbTiO_3$ solid solutions. *Phys. Rev. Lett.* **2007,** *98*, 107601.
57. Boysen, H., Coherence effects in the scattering from domain structures. *J. Phys.: Condens. Matter* **2007,** *19*, 275206.
58. Chen, J.; Sun, X. Y.; Deng, J. X.; Zu, Y.; Liu, Y. T.; Li, J. H.; Xing, X. R., Structure and lattice dynamics in $PbTiO_3$-$Bi(Zn_{1/2}Ti_{1/2})O_3$ solid solutions. *J. Appl. Phys.* **2009,** *105*, 044105.
59. Stephens, P. W., Phenomenological model of anisotropic peak broadening in powder diffraction. *J. Appl. Crystallogr.* **1999,** *32*, 281-289.
60. Brown, I. D.; Shannon, R. D., Empirical bond-strength bond-length curves for oxides. *Acta Crystallogr., Sect. A* **1973,** *A 29*, 266-282.
61. Altermatt, D.; Brown, I. D., The automatic searching for chemical-bonds in inorganic crystal-structures. *Acta Crystallogr., Sect. B: Struct. Sci.* **1985,** *41*, 240-244.
62. Brown, I. D.; Altermatt, D., Bond-valence parameters obtained from a systematic analysis of the inorganic crystal-structure database. *Acta Crystallogr., Sect. B: Struct. Sci.* **1985,** *41*, 244-247.
63. Brese, N. E.; Okeeffe, M., Bond-valence parameters for solids. *Acta Crystallogr., Sect. B: Struct. Sci.* **1991,** *47*, 192-197.
64. Kingsmith, R. D.; Vanderbilt, D., Theory of polarization of crystalline solids. *Phys. Rev. B* **1993,** 47, 1651-1654.
65. Vanderbilt, D.; Kingsmith, R. D., Electric polarization as

a bulk quantity and its relation to surface charge. *Phys. Rev. B* **1993,** 48, 4442-4455.

66. Zhong, W.; Kingsmith, R. D.; Vanderbilt, D., Giant LO-TO Splitting in Perovskite Ferroelectrics. *Phys. Rev. Lett.* **1994,** 72, 3618-3621.

67. Saghi-Szabo, G.; Cohen, R. E.; Krakauer, H., First-principles study of piezoelectricity in $PbTiO_3$. *Phys. Rev. Lett.* **1998,** 80, 4321-4324.

68. Nishida, K.; Kasai, S.; Tanaka, K.; Sakabe, Y.; Ishii, F.; Oguchi, T., First-principle studies on elastic properties and spontaneous polarizations of $PbTiO_3$. *Jpn. J. Appl. Phys.* **2001,** 40, 5806-5808.

69. Sani, A.; Hanfland, M.; Levy, D., The equation of state of $PbTiO_3$ up to 37 GPa: a synchrotron x-ray powder diffraction study. *J. Phys.: Condens. Matter* **2002,** *14*, 10601-10604.

70. Belik, A. A.; Yamauchi, T.; Ueda, H.; Ueda, Y.; Yusa, H.; Hirao, N.; Azuma, M., Absence of Metallic Conductivity in Tetragonal and Cubic $PbVO_3$ at High Pressure. *J. Phys. Soc. Jpn.* **2014,** *83*, 074711.

71. Gröting, M.; Hayn, S.; Albe, K., Chemical order and local structure of the lead-free relaxor ferroelectric $Na_{1/2}Bi_{1/2}TiO_3$. *J. Solid State Chem.* **2011,** 184, 2041-2046.

72. Jiang, B.; Grande, T.; Selbach, S. M., Local Structure of Disordered $Bi_{0.5}K_{0.5}TiO_3$ Investigated by Pair Distribution Function Analysis and First-Principles Calculations. *Chem. Mater.* **2017,** 29, 4244-4252.

73. Gröting, M.; Albe, K., Comparative study of A-site order in the lead-free bismuth titanates $M_{1/2}Bi_{1/2}TiO_3$ (M = Li, Na, K, Rb, Cs, Ag, Tl) from first-principles. *J. Solid State Chem.* **2014,** 213, 138-144.

74. Schäufele, A. B.; Härdtl, K. H., Ferroelastic properties of lead zirconate titanate ceramics. *J.Am. Ceram. Soc.* **1996,** *79*, 2637-2640.

Table of Contents artwork